

# On the role of hand synergies in the optimal choice of grasping forces

M. Gabbicini · A. Bicchi · D. Prattichizzo · M. Malvezzi

Received: 22 November 2010 / Accepted: 30 June 2011 / Published online: 28 July 2011  
© Springer Science+Business Media, LLC 2011

**Abstract** Recent work on the analysis of natural and robotic hands has introduced the notion of *postural synergies* as a principled organization of their complexity, based on the physical characteristics of the hand itself. Such characteristics include the mechanical arrangements of joints and fingers, their couplings, and the low-level control reflexes, that determine the specific way the concept of “hand” is embodied in a human being or a robot. While the focus of work done so far with postural synergies has been on motion planning for grasp acquisition, in this paper we set out to investigate the role that different embodiments have on the choice of grasping forces, and on the ultimate quality of the grasp. Numerical results are presented showing quantitatively the role played by different synergies (from the most fundamental to those of higher-order) in making a number of different grasps possible. The effect of number and types of engaged synergies on the distribution of optimal grasp forces is considered. Moreover, robustness of results is investigated with respect to variation in uncertain parameters such as contact and joint stiffness.

**Keywords** Postural hand synergies · Force closure · Optimal grasping forces

---

M. Gabbicini (✉)  
Interdept. Research Center “E. Piaggio” and DIMNP, University of Pisa, Via Diotisalvi 2, 56122 Pisa, Italy  
e-mail: [m.gabbicini@ing.unipi.it](mailto:m.gabbicini@ing.unipi.it)

A. Bicchi  
Interdept. Research Center “E. Piaggio”, University of Pisa, Via Diotisalvi 2, 56122 Pisa, Italy

D. Prattichizzo · M. Malvezzi  
Department of Information Engineering, University of Siena, Via Roma 56, 53100 Siena, Italy

## 1 Introduction

Recent advances in neuroscience research have shown that the description of how the human hand moves during grasping is dominated by trajectories in a configuration space of much smaller dimension than the kinematic count would suggest. Such configuration space is sometimes referred to as the space of *postural synergies*, or the *eigengrasp space*.

One of the explanations for human efficiency in selecting appropriate grasps is that humans somehow unconsciously simplify the large search space through learning and experience. In a developmental perspective, it can be conjectured that learning is applied to a series of inner representations of the hand of increasing complexity, which varies with the experience and the degree of accuracy required. Santello et al. (1998) investigated this hypothesis by collecting a large set of data containing grasping poses from subjects that were asked to shape their hands in order to mime grasps for a large set ( $N = 57$ ) of familiar objects. Principal Components Analysis (PCA) of this data revealed that the first two principal components account for more than 80% of the variance, suggesting that a very good characterization of the recorded data can be obtained using a much lower-dimensional subspace of the hand DoF space. These and similar results seem to suggest that, out of the ca. 20 DoFs of a human hand, only two or three combinations can be used to shape the hand for basic grasps used in everyday life. It might also be speculated that higher order synergies can be recruited for executing more complex tasks, such as adaptive grasp force control, fine manipulation or haptic exploration.

One first explanation of the observed inter-digit coordination could be advanced in terms of mechanical constraints in the anatomy of the hand. More refined approaches recognize the role of peripheral and central nervous systems in

establishing sensory-motor control synergies, as discussed, e.g., in Mason et al. (2001) and Cheung et al. (2005). Currently, investigations in the role and origin of synergies are being actively pursued by neuroscientists.

What the current knowledge about the neurophysiology of human hands already suggests at this point is that the brain uses the *hand*—meant as a cognitive entity for the organ of the sense of active touch—not as a mere collection of articular joints and muscles, but rather as an organized and ordered ensemble. The organization is dictated by principles that are embedded in the hand’s embodiment—i.e. in its physical characteristics such as the mechanical arrangements of joints and fingers, their couplings, and the low-level control reflexes.

These ideas can be brought to use in robotics, as they suggest a new and principled way of simplifying the design and analysis of hands (as opposed to many empirical, often arbitrary design attempts), which has been the main roadblock for research in artificial hands in the past (Bicchi 2000).

The application of synergy concepts has been pioneered in robotics by Ciocarlie et al. (2007) and Brown and Asada (2007). In Ciocarlie et al. (2007), and later on in Ciocarlie and Allen (2009), the idea has been exploited in the dimensionality reduction of the search space in problems of automated grasp synthesis, and has been applied effectively to derive pre-grasp shapes for a number of complex robotic hands. In Brown and Asada (2007), authors designed a mechanical hand in which more or less accurate actuators are connected to different groups of mechanically interconnected joints, with a priority inspired by resemblance to postural synergies observed in human hands.

Much remains to be done to understand and exploit the implications of the synergy approach to analysis and design of artificial hands. For instance, the role of synergies in fine manipulation and haptic exploration are completely unexplored at present. Very little is known even about all grasping phases subsequent to grasp pre-shaping and contact acquisition, most notably on grasp force distribution and the fundamental problems of form and force closure.

In this paper, we study the effect of the number and type of engaged synergies on the distribution of optimal grasp forces and on the ultimate quality of the grasp.

To investigate grasp force distribution problems in basic whole-hand grasps executed by a hand with a limited number of (synergistic) DoFs, the analytical approach followed by the majority of grasp force studies, which abstract their analysis from the specific physical characteristics of the grasping hand, is unsuitable. We therefore introduce a novel analytical framework, which draws upon previous work on underactuated grasps. Numerical results are presented showing quantitatively the role played by different synergies (from the most fundamental to those of higher-order) in making possible a number of different grasps. As

the analysis method we propose to solve force indeterminacies in the rigid-body system introduces a model of compliance in the system, an issue may arise of how strongly our results depend on a fundamentally uncertain and varying parameter such as compliance. To partially address this problem, we show that our numerical results are quite robust with respect to such uncertainties.

## 2 Preliminaries: Quasi-static manipulation model

### 2.1 Rigid multibody model

We model a cooperating manipulation system as a collection of an arbitrary number of robot “fingers” (i.e., simple chains of links connected through revolute joints) attached to a common base “palm”, and an object, which is in contact with all or some of the links. With reference to Fig. 1 and adopting the notation in Table 1, let  $k$  be the number of fingers,  $n_i$  the number of degrees of freedom for the  $i$ th finger, and set  $n = \sum_{i=1}^k n_i$  as the total number of hand degrees of freedom (DoFs). Moreover, let  $q \in \mathbb{R}^n$  be the vector of joint angles for the whole hand,  $q_i \in \mathbb{R}^{n_i}$  that for the  $i$ th finger, and  $q_{ij} \in \mathbb{R}$  the angle of the  $j$ th limb on the  $i$ th finger.

Adopting the notation introduced in Table 1, the *balance* and *congruence equations* for the object can be respectively written as

$$w_e = Gf, \tag{1}$$

$$\xi_o = G^T \xi_e, \tag{2}$$

where  $G \in \mathbb{R}^{6 \times c}$  is the grasp matrix.

Similarly, the *balance* and *congruence equations* for the hand are, respectively,

$$\tau = J^T f, \tag{3}$$

$$\xi_f = J\dot{q}, \tag{4}$$

where  $J \in \mathbb{R}^{c \times n}$  is the hand Jacobian.

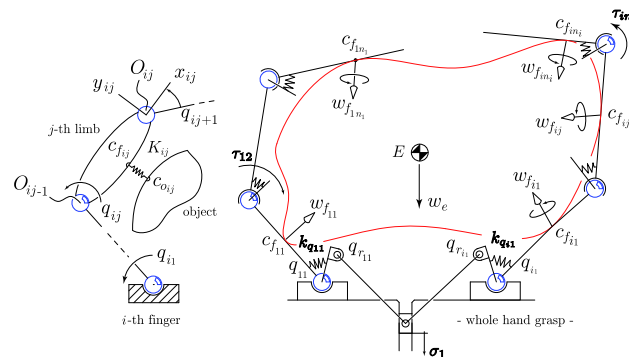


**Fig. 1** Schematic of whole-limb manipulation with synergies. Here, the two-fingered hand is controlled by a single synergy “knob”  $\sigma_1$ , and only some of the limbs make contact with the object

**Table 1** Notation for grasp analysis with postural synergies

| Notation                        | Definition                                      |
|---------------------------------|---|
| P                               | Palm (inertial) frame                           |
| $S_{ij}$                        | D.-H. limb frame, $i$ th finger, $j$ th limb    |
| $L_{ij}$                        | Local limb frame, $i$ th finger, $j$ th limb    |
| $C_{ij}$                        | Local contact frame, $i$ th finger, $j$ th limb |
| E                               | Object frame                                    |
| $n$                             | Number of hand joints                           |
| $q \in \mathbb{R}^n$            | Actual joint angles                             |
| $q_r \in \mathbb{R}^n$          | Reference joint angles                          |
| $\tau \in \mathbb{R}^n$         | Joint torques                                   |
| $s$                             | Number of postural synergies                    |
| $\sigma \in \mathbb{R}^s$       | Synergistic displacements                       |
| $\eta \in \mathbb{R}^s$         | Synergistic generalized forces                  |
| $c$                             | Dimension of the contact force/torque vector    |
| $f$                             | Contact force/torque vector                     |
| $\xi_f \in \mathbb{R}^c$        | Twists of the contact points on the fingers     |
| $\xi_o \in \mathbb{R}^c$        | Twists of the contact points on the object      |
| $u \in \mathbb{R}^6$            | Position and orientation of the object          |
| $\xi_e \in \mathbb{R}^6$        | Object twist                                    |
| $w_e \in \mathbb{R}^6$          | Object wrench                                   |
| $J \in \mathbb{R}^{c \times n}$ | Hand Jacobian matrix                            |
| $S \in \mathbb{R}^{n \times s}$ | Synergy matrix                                  |
| $G \in \mathbb{R}^{6 \times c}$ | Grasp matrix                                    |

For the reader's convenience, a careful exposition of the needed reference frames and a detailed derivation of (1)–(4) can be found in the [Appendix](#).

## 2.2 Introducing elasticity

Now, with reference to taxonomy in Prattichizzo and Trinkle (2000), in order to handle statically-indeterminate or *hyperstatic* grasps, which occur when  $\mathcal{N}(G) \cap \mathcal{N}(J^T) \neq 0$ , we follow Bicchi (1994), and introduce a set of virtual springs at the interface between corresponding contact points  $c_{fij}$  and  $c_{oij}$  on the fingers and the object. These give raise to a system of *linear* constitutive equations linking the components of relative displacements  $\delta\xi_{of} := \delta\xi_o - \delta\xi_f$ , that violate the contact constraints, to the corresponding contact force

$$f = f_0 + \delta f, \quad \delta f = K \delta \xi_{of}, \quad (5)$$

where  $f_0$  is the contact force in the reference configuration  $\delta\xi_o = \delta\xi_f = 0$ . According to Cutkosky and Kao (1989), the stiffness matrix  $K \in \mathbb{R}^{c \times c}$  can be computed as

$$K = (C_s + J C_q J^T)^{-1}, \quad (6)$$

where  $C_s \in \mathbb{R}^{c \times c}$  is the structural compliance matrix (due to, e.g., the flexibility of limbs and fingerpads), and with  $C_q \in \mathbb{R}^n$  the diagonal matrix whose element in position  $(k, k)$  is the compliance at the  $k$ -th joint. Joint compliance in animals is determined by the elastic properties of muscles and tendons and by modulation of the stretch reflex. Similar roles in robot hands are played by transmission and actuator compliance, and by the gain of the  $k$ th position servo. It should be noticed that in both cases joint compliance can be varied, both intentionally and not, although not necessarily in an independent way from joint to joint. Without loss of generality, the matrices  $C_s$  and  $C_q$  employed for the numerical tests reported in this paper are assumed as

$$C_s = (1/k_{\text{stru}})I_{c \times c}, \quad C_q = (1/k_{\text{ss}})I_{n \times n}, \quad (7)$$

where  $k_{\text{stru}}$  (N/mm) is the structural stiffness, while  $k_{\text{ss}}$  (Nmm/rad) is the stiffness of a single joint.

## 3 The “softly underactuated” model

Consideration of synergies introduces a new vista on the grasp problem. A direct interpretation of the results described in Santello et al. (1998) would imply that the joint configuration vector  $q$  could be represented as a function of fewer elements, collected in a *synergy vector*  $\sigma \in \mathbb{R}^s$ , as  $q = q(\sigma)$ , which effectively constrains the hand configuration in an  $s$ -dimensional sub-manifold of the joint configuration manifold. Synergistic hand velocities would belong to the tangent bundle for this manifold, and could be locally described by a linear map  $\dot{q} = S(\sigma)\dot{\sigma}$ . This situation is illustrated in Fig. 2, panels (a)–(d), where the reference posture of the hand is reported as a function of the synergy coefficient  $\sigma_1$  scaling the first synergy vector  $S_1$ .

However, the sole kinematic model of the hand fails to describe the actual grasp of an object (Fig. 2, panels (e)–(h)). Therefore, contact forces must be brought into play if a realistic grasp analysis is in order.

Taking a step further, and in view of dealing with the most general case of statically-indeterminate grasps, both contact and joint compliances have to be included in the analysis.

Therefore, in the model we propose, the synergistic hand displacements  $\delta\sigma \in \mathbb{R}^s$  do not command the joint displacements  $\delta q \in \mathbb{R}^n$  *directly*, as assumed in the analysis in Ciocarlie and Allen (2009) and implemented in the design in Brown and Asada (2007). Instead, the synergistic displacements input  $\delta\sigma$  command the joint reference positions  $q_r$ , as described by the following linear equations (see also Fig. 1)

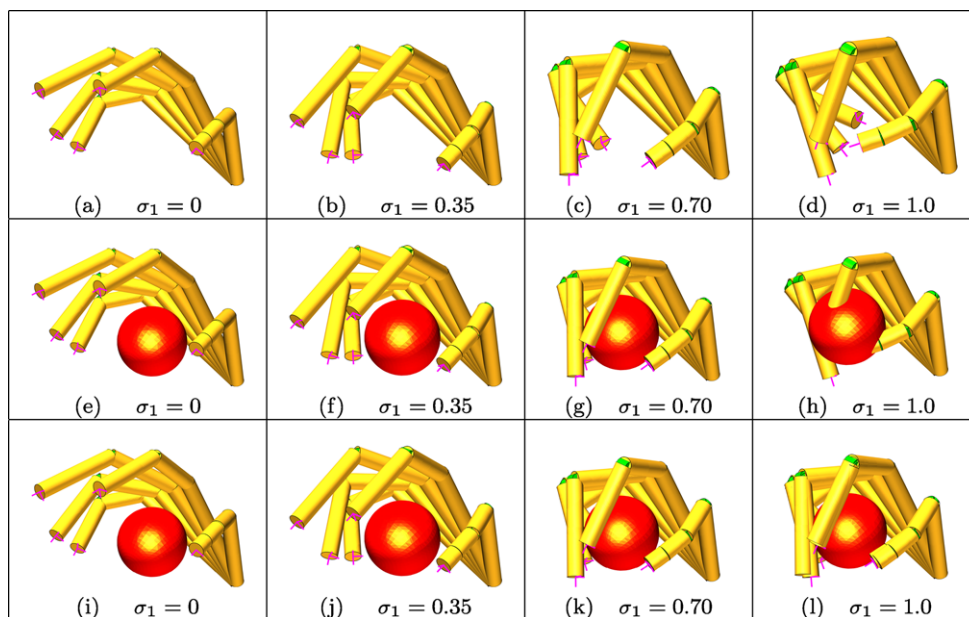
$$\delta q_r = S \delta \sigma, \quad S \in \mathbb{R}^{n \times s} \quad (1 \leq s \leq n). \quad (8)$$

The joint reference positions, in turn, are related to the actual joint displacements by the constitutive equation

$$\delta q = \delta q_r - C_q \delta \tau, \quad (9)$$

where  $C_q$  is the joint compliance introduced in (7).

**Fig. 2** Effect of the first synergy  $S_1$  on the hand posture as a function of the normalized synergy coefficient  $\sigma_1 \in [0, 1]$ . Figs. (a)–(d): reference motion of the hand. Figs. (e)–(h): motion of the hand without contact interaction. Figs. (i)–(l): motion of the hand with contact interaction and joint elasticity



Therefore, the posture (kinematic) synergy model only rules an internal “reference” representation of the hand configuration, and the higher level control of the hand commands this internal representation within the synergy manifold. The actuator system of the hand is controlled towards this reference hand set-point. Then, the hand fingers and palm interact with the manipulated objects and the environment through contacts, and the physical hand reaches an equilibrium under the effects of: attraction towards the synergy-driven reference hand, repulsion by contact forces, stiffness of actuators, tendons, and deformable bodies.

It is worth mentioning that this model, whereby motion is controlled by a reference position and modulation of joint stiffness, has apparent similarities with the *equilibrium point hypothesis* in the motor control literature (Feldman and Levin 2009).

In the pre-grasp phase, forces are null  $\delta\tau = 0$ , hence  $\delta q = \delta q_r$  and the reference and actual posture of the hand overlap perfectly (first three columns in Fig. 2). Hence, in this approach phase, the rigid synergy model  $q = q(\sigma)$  is valid. When an actual grasp of an object occurs, however, the interference (contact) forces and hand compliance cause the actual hand to deviate from the reference hand (panel (l) in Fig. 2). Thus, in our model, the actual hand configuration is driven by synergies, but modifies its posture according to the object shape and compliance. We denote this as a *soft synergy* model of hands.

In the following, we employ the data recorded in Santello et al. (1998) and the definition of finger coordination patterns defined through PCA, to obtain numerical values for the *synergy matrix*  $S$  (also known as “eigengrasp matrix”, Ciocarlie and Allen 2009). More specifically, different simplified synergy matrices  $S$  can be obtained by extracting

a number of columns from the orthogonal *full synergy matrix*  $\tilde{S} \in \mathbb{R}^{n \times n}$  obtained from PCA data, and whose columns are ordered according to the relative contribution to the variance. Each of these extracted synergy matrices will be used as a model of a specific (underactuated) hand.

For later use in Sect. 5, let us further introduce the *balance* equation

$$\eta := S^T \tau = S^T J^T f, \tag{10}$$

where  $\eta \in \mathbb{R}^s$  are the generalized *synergistic forces* corresponding to synergistic displacements.

After modeling the soft synergies, we shift our attention onto the effect of introducing motion coordination patterns for fingers on the ability of the hand to exert internal forces actively (full derivation of the analytical results is omitted for brevity).

### 3.1 General solution of the grasping problem with synergies

Extending the work Bicchi (1994), it can be shown that for a general grasping system with elastic contacts that applies a wrench  $w_e$  to the object, the general solution to the force distribution problem is given by

$$f = G_K^R w_e + \delta f_{hr_s} + \delta f_{ho_s}, \tag{11}$$

$$\delta f_{hr_s} = E_s y, \quad \delta f_{ho_s} = P_s z,$$

where  $G_K^R = K G^T (G K G^T)^{-1} \in \mathbb{R}^{c \times 6}$  is the  $K$ -weighted pseudoinverse of  $G$ , providing the *particular solution*  $G_K^R w_e$  that minimizes the potential energy  $\frac{1}{2} \delta \xi_{of}^T K \delta \xi_{of}$ , (see Hanafusa and Asada 1997; Joh and Lipkin 1991). In (11), the

columns of matrix  $E_s \in \mathbb{R}^{c \times e_s}$  form a basis for the range space of the matrix  $F_s \in \mathbb{R}^{c \times s}$ , mapping the  $\delta\sigma$ 's into the *active internal forces*  $\delta f_{hr_s}$  that can be commanded by synergistic displacements

$$\delta f_{hr_s} = F_s \delta\sigma, \quad F_s := FS, \text{rank}(F_s) = e_s. \tag{12}$$

The matrix  $F \in \mathbb{R}^{c \times n}$  has expression

$$F := (I - G_K^R G)KJ, \quad \text{rank}(F) = e, \tag{13}$$

and maps independently controlled joint reference displacements  $\delta q_r$ 's into *active internal forces*

$$\delta f_{hr} = F \delta q_r. \tag{14}$$

It is worth noting that if all the DoFs of the hand are independently controlled,  $\delta q_r = \delta\sigma$ ,  $S = I \in \mathbb{R}^{n \times n}$ , and (12) reduces to (14). Furthermore, note that for simplicity the force distribution analysis here presented disregards the geometric effects on contact force due to the change of postures of the object and the hand (Chen 2000).

The expression for  $\delta f_{hr_s}$  in (11) is a parameterized version of the active homogeneous solution: optimal grasp force distributions can be found by minimizing a cost function with respect to  $y \in \mathbb{R}^{e_s}$ .

The third term  $\delta f_{ho_s}$  in (11) is a fixed homogeneous solution representing *internal, passive (preload) contact forces*: this corresponds to contact forces that are preloaded at the beginning of the grasp operation (in the rest of the paper it will be assumed  $z = 0 \in \mathbb{R}^{p_s}$ ). Matrix  $P_s \in \mathbb{R}^{c \times p_s}$  represents a basis for this subspace. When all the hand joints are independently controlled, the basis matrix is denoted by  $P \in \mathbb{R}^{c \times p}$ , where  $p$  is the dimension of this subspace.

We summarize the above results by introducing the following subspaces

$$\mathcal{F}_h = \mathcal{R}(A) = \mathcal{N}(G) \subset \mathbb{R}^c, \tag{15}$$

$$\mathcal{F}_{hr_s} = \mathcal{R}(E_s) = \mathcal{N}(G) \cap (\mathcal{R}(KJS) + \mathcal{R}(KG^T)), \tag{16}$$

$$\mathcal{F}_{ho_s} = \mathcal{R}(P_s) = \mathcal{N}(G) \cap \mathcal{N}((JS)^T), \tag{17}$$

that yields the natural decomposition

$$\mathcal{F}_{h_s} = \mathcal{F}_{hr_s} \oplus \mathcal{F}_{ho_s}, \quad \mathbb{R}^c = \mathcal{F}_{h_s} \oplus \mathcal{R}(G_K^R). \tag{18}$$

In case of independent joint control ( $S = I \in \mathbb{R}^{n \times n}$ ), active and passive subspaces in (15) reduce to  $\mathcal{F}_{hr}$  and  $\mathcal{F}_{ho}$ , respectively, as in Bicchi (1994).

It is worth noting that among the free vectors  $y \in \mathbb{R}^{e_s}$ ,  $\hat{y}$  will denote a particular choice corresponding to an optimal grasp force distribution with respect to a chosen cost function.

From a computational point of view, the calculation of the desired basis matrix  $E_s = \text{colbasis}(F_s)$ <sup>1</sup> from (12) is not optimal, since it entails the explicit calculation of  $G_K^R$ . A more efficient algorithm can be obtained by intersection of subspaces, observing that a consistent set of internal forces, parameterized by  $x \in \mathbb{R}^h$ , synergy displacements  $\delta\sigma \in \mathbb{R}^s$ , and object motions  $\delta\xi_e \in \mathbb{R}^6$ , must belong to the nullspace of  $Q_s \in \mathbb{R}^{c \times (h+s+6)}$  (whose nullity is  $b_s$ ), i.e.,

$$\underbrace{\begin{bmatrix} A & -KJS & KG^T \end{bmatrix}}_{Q_s} \begin{bmatrix} x \\ \delta\sigma \\ \delta\xi_e \end{bmatrix} = 0. \tag{19}$$

Defining  $B_s \in \mathbb{R}^{(h+s+6) \times b_s}$ , such that  $\mathcal{R}(B_s) = \mathcal{N}(Q_s)$ , and partitioning  $B_s$  as

$$B_s = [B_{s_1}^T \ B_{s_2}^T \ B_{s_3}^T]^T, \tag{20}$$

where  $B_{s_1} \in \mathbb{R}^{h \times b_s}$ ,  $B_{s_2} \in \mathbb{R}^{s \times b_s}$ , and  $B_{s_3} \in \mathbb{R}^{6 \times b_s}$ , such that

$$\begin{bmatrix} x^T & \delta\sigma^T & \delta\xi_e^T \end{bmatrix}^T = [B_{s_1}^T \ B_{s_2}^T \ B_{s_3}^T]^T \gamma, \quad \gamma \in \mathbb{R}^{b_s}, \tag{21}$$

the subspace of active internal forces can be profitably obtained as

$$\mathcal{F}_{hr_s} = \mathcal{R}(AB_{s_1}), \quad E_s := \text{colbasis}(AB_{s_1}). \tag{22}$$

The synergy displacements  $\delta\hat{\sigma}$  that must be commanded if a desired internal force  $\delta\hat{f} = E_s\hat{y}$  is to be applied are given by

$$\delta\hat{\sigma} = B_{s_2}(AB_{s_1})^+ E_s\hat{y}. \tag{23}$$

According to (8) and (23), the joint reference position is displaced by

$$\delta q_r = SB_{s_2}(AB_{s_1})^+ E_s\hat{y}, \tag{24}$$

and the object moves to a new equilibrium position defined by

$$\delta\xi_e = B_{s_3}(AB_{s_1})^+ E_s\hat{y}. \tag{25}$$

Due to contact forces in the interaction with the object and the joint compliance, the hand joints moves differently with respect to the commanded reference, i.e.,  $\delta q \neq \delta q_r$ . Their values can be explicitly calculated as

$$\delta q = [I - C_q J^T (I - G_K^R G)KJ]S\delta\hat{\sigma}, \tag{26}$$

where  $\delta\hat{\sigma}$  can be recovered from (23). It is worth observing that in case of perfectly rigid joints,  $C_q = 0 \in \mathbb{R}^{n \times n}$ , and

<sup>1</sup>The operator  $\text{colbasis}(F_s)$  returns a basis for the column space of the input matrix  $F_s$ .

$\delta q = \delta q_r$ . The other quantities are also modified due to the increased global stiffness, as evident from the definition of  $K$  in (6).

Finally, corresponding variation of the joint torques  $\delta \tau$  can be obtained as

$$\delta \tau = J^T (I - G_K^R G) K J S \delta \hat{\sigma}, \tag{27}$$

and the associated variation of the synergistic forces  $\delta \eta$  is

$$\delta \eta = S^T \delta \tau. \tag{28}$$

### 3.2 Qualitative analysis of hand embodiment

With reference to (12), the following relationships between ranks hold

$$\underbrace{\text{rank}(F_s)}_{e_s} = \underbrace{\text{rank}(S)}_s - \dim(\mathcal{N}(F) \cap \mathcal{R}(S)), \tag{29}$$

$$\text{rank}(F_s) \leq \min\{\text{rank}(F), \text{rank}(S)\}, \tag{30}$$

$$\text{rank}(F_s) \geq \text{rank}(F) + \text{rank}(S) - n. \tag{31}$$

Therefore, under the condition that each synergy  $S_i$  ( $i \in \mathcal{S}$ )<sup>2</sup> has a non-null projection onto  $\mathcal{R}(F^T)$ , we can assume that  $e_s = s$ . In this case, consider a fully actuated grasp with  $\text{rank}(F) = e$ . For the same grasp, consider underactuation and increase one by one the number of the engaged columns of  $S$ . As the number of synergies engaged increases, say  $1 \leq s \leq e$ , the dimension of the subspace  $\mathcal{F}_{hr_s}$  of active internal forces also increases in the same manner. For  $s > e$ , according to (30),  $e_s = e$ , and the dimension of the subspace  $\mathcal{F}_{hr_s}$  reaches a plateau. This means that for fully actuated grasping systems characterized by an  $e$ -dimensional  $\mathcal{F}_{hr}$ , underactuation with a number of synergies  $s \sim e$  does not endanger the ability to exert the *same* internal forces. If  $e$  is “small”, say e.g.  $s = 2$  or  $s = 3$ , application of an equally “small” number of synergies  $s$  results in a great control simplification without side effects on the grasping ability of the system, see results in Sect. 5.3.

A fundamental issue we want to investigate is the link between basic synergies, i.e., the first components obtained via PCA, accounting for much of the variance in geometric posture space, and the ability of the corresponding underactuated system to firmly grasp an object. However, the sole rank count in (29) does not allow to compare *quantitatively* synergies with different shapes, i.e., different columns of  $S$ . Therefore, in this analysis the behaviour of a system underactuated by means of different number of synergies and, once fixed their number, with different synergies  $S_i$ , is presented. The performance parameter is the ability to attain

*force-closure* conditions and, if this is the case, in obtaining lower values of a suitably defined cost function in determining optimal grasping forces. Then, we discuss robustness issues with respect to variations of the grasping stiffness: the range, going from values typical of robotic hands to those of the human hand, is elicited from Kao et al. (1997), and Friedman and Flash (2007).

## 4 Force-closure problem with synergies

At an intuitive level, the meaning of “force-closure” is that motions of the grasped object are completely restrained against arbitrary external disturbances, by virtue of the contact forces that the hand is capable to exert on the object. We emphasize here that this definition is very relevant to synergistically (under)actuated hands. Indeed (as opposite to the purely geometric nature of form-closure), force-closure involves consideration of which contact forces can be actively applied on the object by the specific hand under consideration. Under this regard, it clearly makes a difference if an object is grasped by a hand controlled by different numbers and types of synergies (corresponding to different active internal force subspaces, as discussed in the previous section).

Accordingly, we adopt here the definition of force-closure given in Bicchi (1995), which considers the case of underactuated hands:

**Definition 1** (Force-Closure) A grasp is defined Force-Closure if and only if the following conditions are satisfied:

1. Forces in arbitrary directions are resistible, i.e.  $\text{rank}(G) = 6$ .
2. The hand configuration is prehensile, i.e.  $\exists y$  such that  $f(y) \in \text{Int}(\mathcal{F})$ ,<sup>3</sup> with  $f(y) = Ey$ .

In Definition 1,  $\mathcal{F}$  is the composite friction cone defined as  $\mathcal{F} = \mathcal{F}_{11} \times \dots \times \mathcal{F}_{k,n_k}$ . For brevity, we recall here only those types of friction cone implemented in our software, used to carry out numerical results in later sections. For a point contact with friction (PCWF), we have  $f_{ij} \in \mathbb{R}^3$  and

$$\mathcal{F}_{ij} = \left\{ f_{ij} \in \mathbb{R}^3 \mid f_{ij_3} \geq 0, \frac{1}{\mu_{ij}}(f_{ij_1}^2 + f_{ij_2}^2) \leq f_{ij_3}^2 \right\}, \tag{32}$$

where  $f_{ij_3}$  is the normal component of the contact force at the point of contact  $c_{ij}$ ,  $f_{ij_1}$ ,  $f_{ij_2}$  the components in the tangential directions, and  $\mu_{ij}$  the Coulomb friction coefficient.

For a soft-finger with elliptical friction limit approximation (Buss et al. 1996), we have  $f_{ij} \in \mathbb{R}^4$  and

$$\mathcal{F}_{ij} = \left\{ f_{ij_3} \geq 0, \frac{1}{\mu_{ij}}(f_{ij_1}^2 + f_{ij_2}^2) + \frac{1}{\mu_{ij_t}} f_{ij_4}^2 \leq f_{ij_3}^2 \right\}, \tag{33}$$

<sup>2</sup> $\mathcal{S}$  is a set of indices used to select the corresponding columns in  $\bar{S}$  to build  $S$ .

<sup>3</sup> $\text{Int}(\mathcal{F})$  denote the internal part of the composite friction cone  $\mathcal{F}$ .

where  $\mu_{ij_i}$  is a proportionality constant between the torsion and shear limits. It is worth noting that the above models do not necessarily assume equal friction coefficients at all contact points: however, for brevity, in the numerical tests reported in Sects. 5.3 and 5.4, the friction coefficients will be assumed constant, i.e.,  $\mu_{ij} = \mu$  and  $\mu_{ij_i} = 1$ .

#### 4.1 Force closure problem as a second order cone programming (SOCP)

In view of formulating and solving the problem as a second order cone programming (SOCP) one, for which efficient algorithms and interfaces are today a mature technology, we recall that the satisfaction of the friction limit constraints in (32) and (33) is equivalent to the positive definiteness of matrix  $P = \text{Blockdiag}(P_{in_i})$ ,  $P \succ 0$ , where the explicit expression for each  $P_{ij}$ , with  $(i = 1, \dots, k; j \in \nu(i))$ , can be found in Buss et al. (1996).

Then, consider the problem of finding the optimal distribution of contact forces  $f$  in the grasp of an object subject to the external load with regard to the minimization of a suitable cost function  $\Psi(y)$ . To formalize this problem, we give the following definition:

**Definition 2** (Grasping Force Optimization) Given a grasp characterized by  $G_W^R$ ,  $E_s$ , and  $P_s$ , and an object wrench  $w_e \in \mathbb{R}^6$ , find  $\hat{y}$  in (11), such that  $f(\hat{y}) \in \text{Int}(\mathcal{F})$ , and the cost function  $\Psi(f(\hat{y}))$  is minimized.

In numerical tests, we assume: (i) zero preload at the beginning of the grasp ( $z = 0$  in (11)); (ii) zero net wrench applied to the object,  $w_e = 0$ ; (iii) an auxiliary constraint on the minimum value for all the normal components  $f_n$  of the contact force. Under these hypotheses, the grasping force optimization problem is set up in the following way

$$\hat{y} = \text{argmin } \Psi(y) \quad (34)$$

subject to  $f = E_s y$ ,  $P(f) \succ 0$ ,  $f_n \geq f_{\min}$ .

Optimal contact force distribution is sought by employing, in turn, each of the following cost functions

$$\Psi_f(y) := \|f(y)\|_2, \quad \Psi_{f_\infty}(y) := \|f(y)\|_\infty,$$

$$\Psi_\tau(y) := \|\tau(y)\|_2, \quad \Psi_\eta(y) := \|\eta(y)\|_2,$$

where  $f \in \mathbb{R}^c$  are the contact forces,  $\tau \in \mathbb{R}^{n_c}$  the joint torques for the contacting fingers in (3), and  $\eta \in \mathbb{R}^s$  the synergistic forces in (10).

The problem is set up and solved as a semidefinite program (SDP) by employing the CVX modeling system for convex optimization based on MATLAB, see Grant and Boyd (2004) and Grant and Boyd (2008) for further details. The solver used is SDPT3 (Toh et al. 1999), which

implements an infeasible path-following algorithm for solving general SQLP—conic optimization problems involving semidefinite, second-order and linear cone constraints.

#### 4.2 Barrier formulation of the force optimization problem

Hitherto, the force closure problem has been setup and solved as a *constrained* minimization problem. An alternative approach, originally proposed in Bicchi (1995) in the force optimization context, suggests the inclusion of the constraints in the cost function  $V(y)$ , according to a barrier strategy (Borgstrom et al. 2010). This can be solved as an *unconstrained* minimization problem as follows

$$\hat{y} = \text{argmin } V(y), \quad (35)$$

whose solution  $\hat{y}$  corresponds to the contact forces  $f(\hat{y})$  maximizing (in the sense to be defined later) the distance from the constraint boundaries. As already described in (4.1), in order to assure the feasibility of the grasp, thus avoiding contact losses and slippage, the contact forces must belong to a nonlinearly bounded set (friction cone). More precisely, in order to fulfill contact constraints, the components of the internal force vector must belong to some nonlinearly bounded subset of the image of  $E$ . In Bicchi (1995) such subset was proven to be convex, and an efficient algorithm to find the internal force set, maximizing the distance from this boundary, has been provided. In Bicchi and Prattichizzo (2000) the algorithm was then generalized for tendinous actuated hands.

For the sake of simplicity, let us assume Hard Finger (PCWF) contact model (in Bicchi and Prattichizzo 2000 the algorithm was generalized also to different contact types). The friction constraint previously introduced in (32) can be expressed by the following inequality:

$$\psi_{ij,f} = \alpha_{ij} \|f_{ij}\| - f_{ij_3} < 0 \quad (36)$$

where  $\alpha_{ij}$  is defined as  $\alpha_{ij} = (1 + \mu_{ij}^2)^{-1/2}$ . If inequality (36) is satisfied, the  $(i, j)$ th contact force lies inside the friction cone. According to (11), the contact forces depend on external wrench  $w$  and on  $y$ .

Other inequalities can be defined in order to constrain the minimum value of the normal component  $f_{ij_3}$  of the contact force

$$\psi_{ij,m} = f_{\min} - f_{ij_3} < 0. \quad (37)$$

Likewise, the maximum value of the contact force norm  $\|f_{ij}\|$  can be reasonably constrained, due to actuator maximum allowable effort or hand structural properties or object strength:

$$\psi_{ij,M} = \|f_{ij}\| - f_{\max} < 0. \quad (38)$$

**Table 2** Force constraint coefficients

| Constraint type               | $\alpha_{ij,k}$ | $\gamma_{ij,k}$ | $\delta_{ij,k}$ |
|-------------------------------|-----------------|-----------------|-----------------|
| Friction cone ( $k = f$ )     | $\alpha_{ij}$   | -1              | 0               |
| Min. normal force ( $k = m$ ) | 0               | -1              | $f_{\min}$      |
| Max. force module ( $k = M$ ) | 1               | 0               | $-f_{\max}$     |

The above constraints (36), (37) and (38) can be rewritten in a more compact form as

$$\psi_{ij,k} = \alpha_{ij,k} \|f_{ij}\| + \gamma_{ij,k} f_{ij_3} + \delta_{ij,k} < 0, \tag{39}$$

where the subscripts  $ij$  refers to the contact point, and the subscript  $k = f, m, M$  refers to the constraint type. The coefficients in the above inequality assume the values reported in Table 2.

In Bicchi and Prattichizzo (2000) other inequalities related to bounding minimum and maximum values of tendon efforts were added: those are not included here for the sake of simplicity.

For a given wrench  $w$ , let us define  $\Omega_{ij,k}^\epsilon$  the set of  $y$  that satisfies (39) with a positive margin  $\epsilon$ :

$$\Omega_{ij,k}^\epsilon = \{y | \psi_{ij,k}(w, y) < -\epsilon\}. \tag{40}$$

Let us then introduce, for the  $(i, j)$ th contact and the  $k$ th constraint, the function

$$V_{ij,k}^\epsilon(w, y) = \begin{cases} (d\psi_{ij,k}^2)^{-1}, & y \in \Omega_{ij,k}^\epsilon, \\ a\psi_{ij,k}^2 + b\psi_{ij,k} + c, & y \notin \Omega_{ij,k}^\epsilon. \end{cases} \tag{41}$$

This function can be made twice continuously differentiable by choosing  $d = 2N^{-2}$ ,  $a = \frac{3}{2\epsilon^4}N^{-2}$ ,  $b = \frac{4}{\epsilon^3}N^{-1}$ ,  $c = \frac{3}{\epsilon^2}$ . Since  $\epsilon$  is dimensionally a force, the coefficients multiplying  $\epsilon^{-4}$ ,  $\epsilon^{-3}$  and  $\epsilon^{-1}$  (i.e.  $\frac{3}{2}$ , 4 and 3) are expressed in  $N^2$ . With the above assumptions for the  $a$ ,  $b$  and  $c$  units,  $V$  is a dimensionless quantity. Furthermore, let us associate to the grasp the function  $V^\epsilon(w, y)$  defined as

$$V^\epsilon(w, y) = \sum_{i,j} \sum_{k=f,m,M} V_{ij,k}^\epsilon(w, y). \tag{42}$$

In Bicchi (1995), the author showed that the function is strictly convex. Indicating with  $\hat{y}$  the (unique) solution of problem (35), the reciprocal of  $V(\hat{y})$  is a well defined force closure quality index that reflects the *distance* of the grasp from violating the constraints (39).

### 5 Numerical tests

#### 5.1 Paradigmatic hand model

The paradigmatic hand model is schematically represented in Fig. 3. This is the *same* model for which detailed data

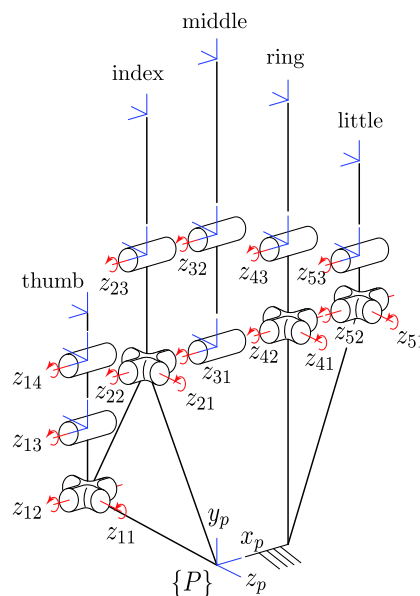


**Fig. 3** 15 DoFs kinematic model of the paradigmatic hand

were collected and presented in Santello et al. (1998). The fact that the large amount of high-quality data taken in Santello et al. (1998) was kindly made available to us is a reason for this choice, along with the motivation that synergies can be defined for no other kinematic structure without a dose of arbitrariness.

Examples of human hand biomechanical models are available in the literature (Lee and Kuni 1995; Lin and Wu 2000; Linscheid et al. 1991). The fingers are usually modeled as kinematic chains independent from each other, sharing only their origin in the hand palm. In absence of disabilities or handicaps, the ratios between the bones lengths of each finger are almost constant (Kim et al. 2002; Youm et al. 1977).

For our analysis, the objective of the kinematical model is to closely copy the properties of the hand rather than its intrinsic structure. The human hand joints can mainly be divided into 1-DoF and 2-DoF joints. The 1-DoF joints in the hand can be represented as revolute joints; the 2-DoF joints can be divided into two types. The *trapeziometacarpal* joint of the thumb is a saddle joint with non-orthonormal axes, the *metacarpophalangeal* joints of the fingers are condyloid. The main difference between saddle and condyloid joints is that condyloid joints have approximately intersecting axes while saddle joints do not. For the thumb, the axes of the metacarpal are non-orthogonal screw.

Therefore the *metacarpophalangeal* joint of the index, middle, ring and little fingers are usually modeled as a two DoFs joint (one for adduction/abduction and another flexion/extension). The *proximal interphalangeal* and *distal interphalangeal* joints of the other fingers can be modeled as a one DoF (revolute) joint. The thumb has at least 5 DoF:

**Table 3** D.-H. tables for the 15 DoFs paradigmatic hand

(a) D.-H. table for the Thumb finger

| Limb     | $a$ (mm) | $\alpha$ (rad) | $d$ (mm) | $q$ (rad) |
|----------|----------|----------------|----------|-----------|
| $l_{11}$ | 0        | $-\pi/2$       | 0        | $q_{11}$  |
| $l_{12}$ | $a_{12}$ | 0              | 0        | $q_{12}$  |
| $l_{13}$ | $a_{13}$ | 0              | 0        | $q_{13}$  |
| $l_{14}$ | $a_{14}$ | 0              | 0        | $q_{14}$  |

(b) D.-H. table for Index, Ring and Little fingers. Indices take the following values:  $i = 2, 4, 5$  and  $j = 1, 2, 3$

| Limb     | $a$ (mm) | $\alpha$ (rad) | $d$ (mm) | $q$ (rad) |
|----------|----------|----------------|----------|-----------|
| $l_{ij}$ | 0        | $-\pi/2$       | 0        | $q_{ij}$  |
| $l_{ij}$ | $a_{ij}$ | 0              | 0        | $q_{ij}$  |
| $l_{ij}$ | $a_{ij}$ | 0              | 0        | $q_{ij}$  |

(c) D.-H. table for the Middle finger

| Limb     | $a$ (mm) | $\alpha$ (rad) | $d$ (mm) | $q$ (rad) |
|----------|----------|----------------|----------|-----------|
| $l_{31}$ | $a_{31}$ | 0              | 0        | $q_{31}$  |
| $l_{32}$ | $a_{32}$ | 0              | 0        | $q_{32}$  |

2 DoF in *trapeziometacarpal* joint, 2 DoF in *metacarpophalangeal* joint, and 1 DoF in *interphalangeal* joint. Anyway, the range of deviation of metacarpophalangeal joint is so small that generally can be modeled as a single DoF joint, while the trapeziometacarpal joint is more important in the analysis of the thumb kinematics (Kim et al. 2002).

Our model has 15 DoFs corresponding to: 4 DoFs for the thumb: TR, TA, TM, TI (Thumb Rotation, Abduction, Metacarpal, Interphalangeal); 3 DoFs for the index: IA, IM, IP (Index Abduction, Metacarpal, Proximal interphalangeal); 2 DoFs for the middle: MM, MP (Middle Metacarpal, Proximal interphalangeal); 3 DoFs for the ring: RA, RM, RP (Ring Abduction, Metacarpal, Proximal interphalangeal); 3 DoFs for the little: LA, LM, LP (Little Abduction, Metacarpal, Proximal interphalangeal). It is worth noting that the middle finger has no abduction since it is considered the “reference finger” in the sagittal plane of the hand. Moreover, the Distal Interphalangeal (DI) angle is not present in none of the four fingers due to the limitation in the sensors embedded in the measuring glove employed, see Santello et al. (1998) and references therein. With  $P = (O_p; x_p, y_p, z_p)$  with indicate the palm frame, and with  $S_{ij} = (O_{ij}; x_{ij}, y_{ij}, z_{ij})$  and  $C_{ij} = (C_{ij}; x_{c_{ij}}, y_{c_{ij}}, z_{c_{ij}})$  the D.-H. and the normalized Gauss frame, respectively, for the  $j$ th limb on the  $i$ th finger. The D.-H. tables for each finger/group of fingers are shown in Tables 3a–3c.

5.2 Assumptions in the definition of grasp layouts

To define possible grasp configurations, we rely on data reported in Santello et al. (1998). In that work, no measure-

**Table 4** Nominal data common to all tests

| Net wrench $w_e$ | Contact type | Frict. coeff. $\mu$ | $f_{\min}(N)$ |
|------------------|--------------|---------------------|---------------|
| 0                | PCWF         | 1.0                 | 0.1           |

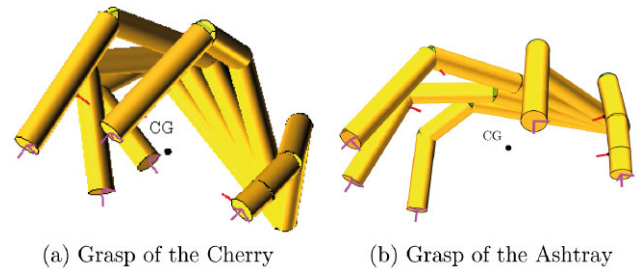


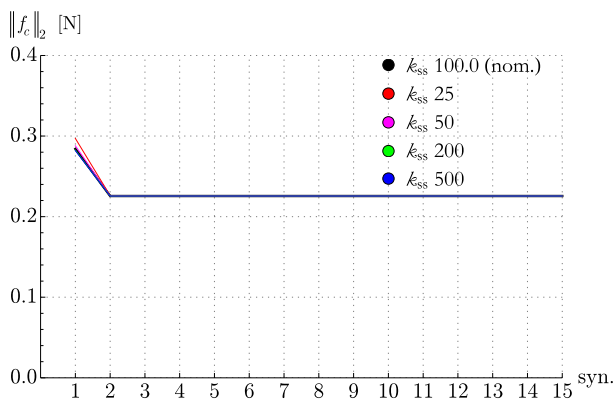
**Fig. 4** Hand postures analyzed

ment of the object position, nor spatial location of the contact points, was registered (since the subjects were asked to shape their hands in order to mime grasps, with no physical object present). Therefore we made the following assumptions. Firstly, the hand configuration relative to the imagined grasp of an object, say a cherry, was defined as the mean joint configuration vector recorded in the grasp of that object, among a total of five trials. Therefore, the configuration of the hand is identified with the name of the object grasped. Secondly, a reasonable position of the center of gravity  $CG$  for the grasped object was defined, taking into account both the hand configuration previously defined and a reasonable shape for that object. Then, the candidate contact point  $c_{f_{ij}}$  on each limb  $l_{ij}$  was found as the nearest point on the same limb to  $CG$ . Last step was to define the final grasp by selecting the limbs in contact, according to both the shape of the hand and the position of the object relative to the hand the same grasp suggests. The numerical data common to all tests are listed in Table 4.

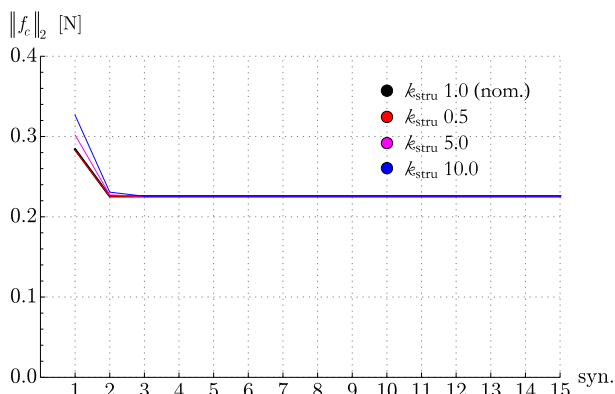
5.3 Precision grasp—the cherry

As a first test case we consider the grasp of a cherry. The hand configuration, the estimated position of the center of gravity  $CG$  of the object and the contact points are represented in Fig. 4a. The contact parameters employed are listed in Table 4 and, with reference to (6) and (7), the numerical value of the stiffness matrix  $K$  is specified by setting  $k_{stru} = 1$  N/mm and  $k_{ss} = 100$  Nmm/rad. For this case,  $\text{rank}(G) = 6$ ,  $c = 9$  and, with reference to (12), (13), and (15),  $h = e = 3$ ,  $p = 0$ . The optimal contact force distribution is found with respect to  $y$  minimizing  $\psi_f(y) = \|f(y)\|_2$ .

Let us concentrate on the black curve in Fig. 5a. Interestingly enough, this grasp is force-closure even when engaging only the first synergy ( $S_1$ , first column of  $S$ ), for



(a) Trends for variation of the steady-state gain  $k_{ss}$  (Nmm/rad).



(b) Trends for variation of the structural stiffness  $k_{stru}$  (N/mm).

**Fig. 5** (Color online) The cherry. Norm of the optimal contact force  $f$  w.r.t. the cost function  $\|f\|_2$ , with increasing number of synergies

which an optimal value of  $\|f\|_2 = 0.284$  N, is found. When more synergies are engaged in the grasp, the norm of the contact force decreases as the dimension  $e_s = s$  of  $\mathcal{F}_{hr_s}$  increases, and there is a higher dimensional space where the optimal solution can be sought. Then, a plateau is obtained once the dimension  $e_s$  reaches  $e$ , as confirmed by rank considerations in (29). Therefore, as far as controllable internal contact forces are concerned, no improvement can be obtained in the quality of the grasp by engaging a number of synergies  $s > e$ .

It is worth stressing that the trend in Fig. 5 is *highly dependent* on which synergies are considered. Had we engaged synergies in a backward fashion, i.e., from  $S_{15}$  to  $S_1$ , we would have obtained a completely different trend. Put another way, if we plug in *only one* synergy at a time, the grasp is force-closure only for synergies  $S_1, S_3$  and  $S_4$ , meaning that maybe the first synergies are more fundamental to grasp objects than those of higher-order, but not in a strictly ordered fashion. However, we have no ambition of drawing general conclusions here, since fundamental roles are played by location of the contact points, surface normals, and types

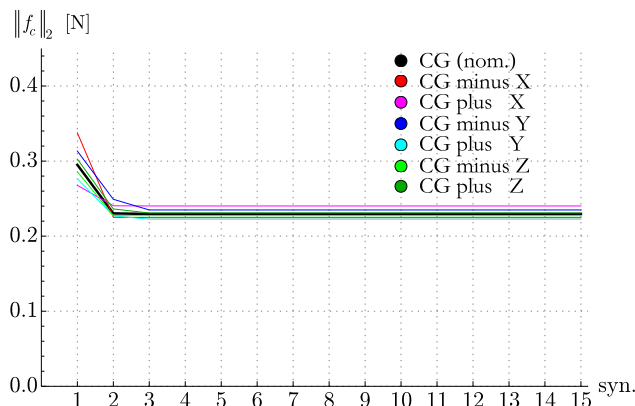


**Fig. 6** (Color online) The cherry. Norm of the optimal contact force  $f$  w.r.t. the cost function  $\|f\|_2$ , with increasing number of synergies—sensitivity on object CG displacement

of contact constraints, which are here only reasonably estimated.

Figure 6 shows the results obtained moving the center of gravity  $CG$  in the  $x, y$  and  $z$  directions and, consequently, changing the contact point positions and the corresponding normal directions. The applied CG displacement is  $\pm 5$  mm. The simulation results show that curve trends are consistent with respect to variations of contact point location.

Figure 7 shows the optimal contact force distribution found with respect to  $y$  minimizing  $\psi_{f_\infty}(y) = \|f(y)\|_\infty$ . Even with this cost function, the grasp is again force-closure when engaging only the first synergy. When more synergies are engaged in the grasp, again a plateau is obtained once the dimension  $e_s$  reaches  $e$ . We observe that the saturation value obtained for  $s \geq e$  is  $\|f\|_\infty = 0.1$  N, that corresponds to the minimum force limit  $f_{min}$  in Table 4.

In order to assess the robustness of the above trends with respect to the grasp stiffness, the previous analyses are repeated for different values of  $K$  obtained varying  $k_{ss}$  and  $k_{stru}$ , as shown in Figs. 5a–5b and Figs. 7a–7b.

Interestingly, if we select  $\Psi_\eta(y) = \eta_2$  as cost function, we obtain the trends depicted in Figs. 8a–8b. These show that, in terms of synergistic forces, adding more synergies than those strictly necessary to fulfill the dimension of  $\mathcal{F}_{hr}$  worsens the cost, as the range of  $S$  (where we project the same  $\tau$ 's, see (10)) increases. In other words, if a synergy is not actuated, synergistic forces in its direction are absorbed by the mechanical structure directly, and are not reflected in actuation costs.

Minimization of  $\Psi_\tau(y) = \tau_2$  bears trends similar to those of Fig. 5, and are here omitted for brevity.

The optimal value  $\hat{y}$  minimizing the function  $V(y)$  in (42) has been analyzed as a function of the number of engaged synergies. The following values have been initially chosen for the constraints:  $\mu = 0.5, f_{min} = 1$  N,  $f_{max} = 30$  N.

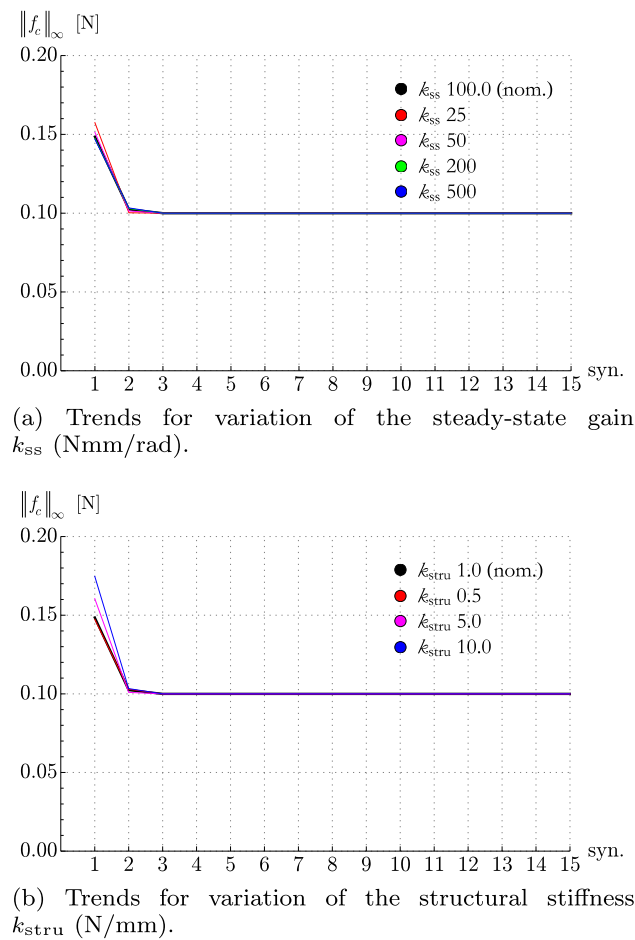


**Fig. 7** (Color online) The cherry. Infinity norm of the optimal contact force  $f$  w.r.t. the cost function  $\|f\|_\infty$ , with increasing number of synergies

The `fminsearch` MATLAB function has been employed. Figure 9a shows the cost  $V$  as a function of the number of engaged synergies. The function decreases for synergies increasing from 1 to 3 and then it remains constant.

Furthermore, for each optimal configuration, the single contributions to  $V$  of each constraint have been evaluated:  $V_k^\kappa = \sum_{ij} V_{ij,k}^\kappa$ . In the same figure, the different curves represent the contributions of each constraint: friction contribution  $V_\mu$ , minimum value of normal component of the contact force  $V_{min}$ , maximum value of contact force magnitude  $V_{max}$ , in order to highlight the relative weight of each constraint. As clearly visible, in the selected configuration, the main contribution in  $V$  is due to the friction constraint  $V_\mu$ .

In order to highlight the contact force *distance* from the friction cone boundary, Fig. 9b shows for each of the three contact points (1-thumb, 2-index, 3-middle), the angle  $\theta_i = \cos^{-1}(f_i^T n_i / \|f_i\|)$  between the contact force and the direction normal to the contact surface, and their sum  $\Theta = \sum_{i=1}^3 \theta_i$ , as a function of the engaged synergies. The qualitative behavior of  $\Theta$  is similar to  $V$ : its value decreases

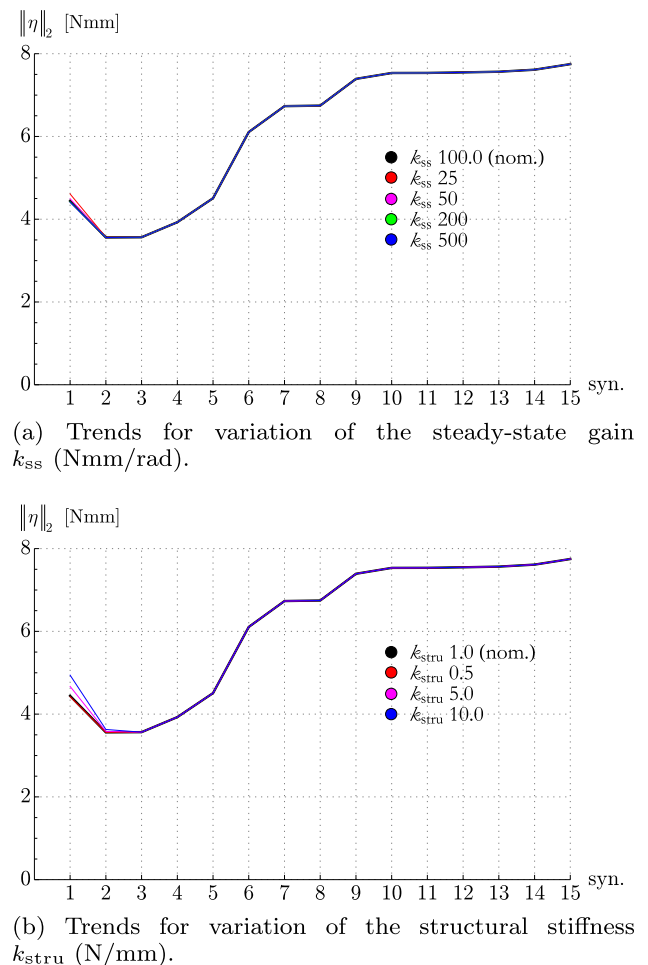
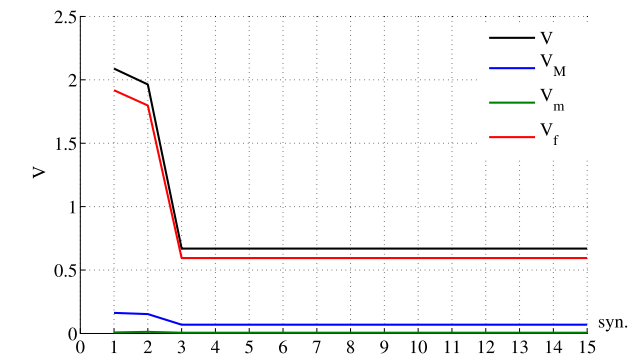


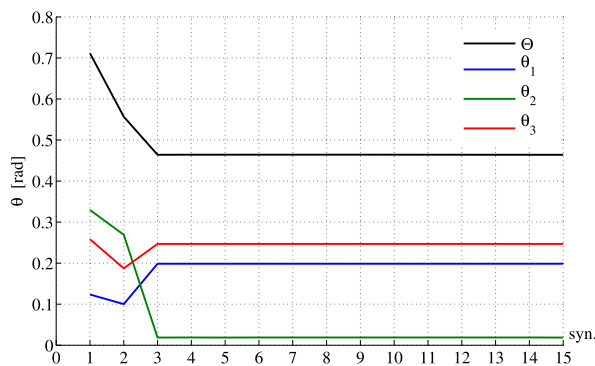
**Fig. 8** (Color online) The cherry. Norm of the optimal synergistic force  $\eta = S^T \tau$  w.r.t. the cost function  $\|\eta\|_2$ , with increasing number of synergies

for synergies increasing from 1 to 3, and then it remains constant. Furthermore, we can observe that, while  $\theta_1$  and  $\theta_3$  are substantially constant,  $\theta_2$  sensibly decreases. This result is evident in Fig. 10, that shows in the  $xy$  projection of the operative hand space, the contact points (red stars), the normal directions (blue arrows) and the optimal contact forces (black arrows) when only the first synergy is engaged (Fig. 10a), and when the first three synergies are activated (Fig. 10b). Of course these *specific* results, relative to each single contact points, are highly depends on hand configuration, contact point location,  $\mu$ ,  $f_{min}$  and  $f_{max}$ , etc.

Furthermore, the weight of each constraint in the cost function  $V$  has been evaluated by analyzing the  $\psi_{ij,k}$  values, Fig. 11. Figure 11a shows the contribution of each type of constraint: in order to simplify the representation, the sum of constraint value for each type is presented. The figure clearly shows that, in the considered configuration, the most critical constraints are related to the friction, since the curve relative to the  $\sum_{i,j} \psi_{ij,f}$  constraints is near to the limit (zero)



(a)  $V(\hat{y})$ ,  $V_\mu$ ,  $V_{\min}$ ,  $V_{\max}$  vs number of engaged synergies.

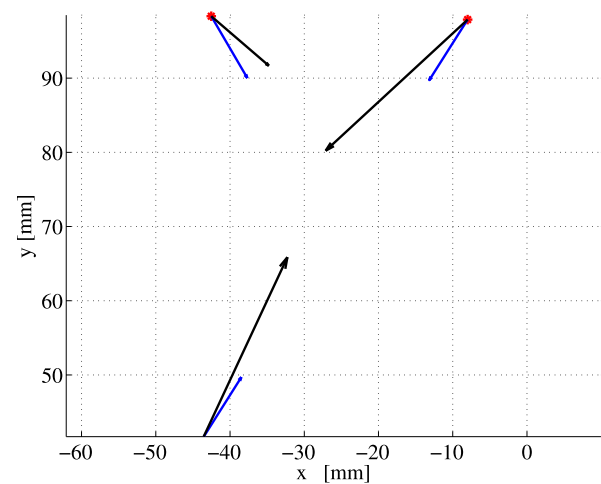


(b)  $\Theta(\hat{y})$ ,  $\theta_1$ ,  $\theta_2$ ,  $\theta_3$  vs number of engaged synergies.

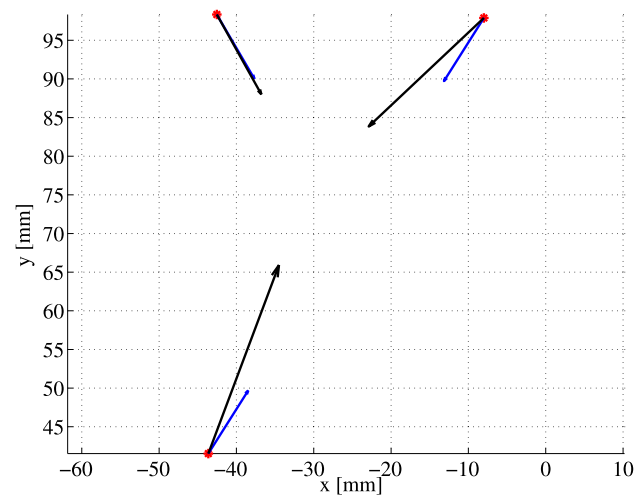
**Fig. 9** (Color online) The cherry. Results of  $V(y)$  minimization as a function of the engaged synergies

value. However, Fig. 11a does not show clearly the effect of the number of engaged synergies: this effect is evident in Fig. 11b, where the single  $\psi_{ij,f}$  components are plotted. By increasing the number of engaged synergy from one to three, the second component (corresponding to the contact point on the index) sensibly decreases, and recalling expression (41), it leads to a significant  $V$  decrease.

A sensitivity analysis was performed in order to study the effect of boundaries  $\mu$ ,  $f_{\min}$  and  $f_{\max}$  on  $V$  for different numbers of engaged synergies. Figure 12a summarizes the effect of the friction coefficient  $\mu$ . We observe that decreasing the value of the friction coefficient, for a given number of engaged synergies, the overall  $V$  values increase, since the friction constraint is more critical. In all the analyzed configurations, increasing the number of synergies from one to three the cost function decreases. Furthermore, increasing the number of actuated synergies the cost function remains constant. Figure 12b shows how the curves  $V$  vs synergies change modifying  $f_{\min}$  values from 1 to 10 N. We observe that increasing the  $f_{\min}$  values, the overall  $V$  increases, since the minimum normal force constraint becomes more important. In Fig. 12c the effect of  $f_{\max}$  value is analyzed. In this case, decreasing  $f_{\max}$  values we observe a  $V$  increase, for



(a) Only the first synergy is engaged.



(b) The first three synergies are engaged.

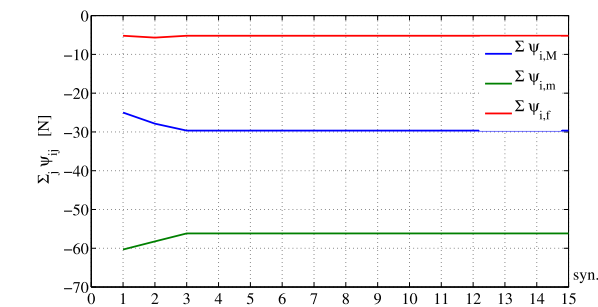
**Fig. 10** (Color online) The cherry. Contact points (red stars), contact normals (blue arrows) and contact forces (black arrows) when only the first synergy is activated and the first three synergies are activated

the same reasons previously explained. Further tests were realized changing  $\epsilon$  value from  $10^{-3}$  N to  $10^{-7}$  N: the results are substantially the same for all the performed tests.

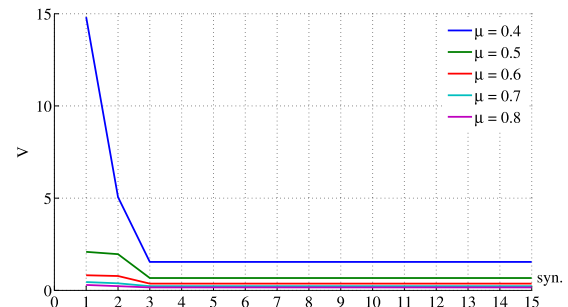
Finally the robustness of the observed  $V$  trends with respect to contact point displacements are shown in Fig. 13. Also in this analysis the obtained  $V$  vs engaged synergies trends are quite consistent with respect to small variation of the contact point positions.

#### 5.4 Power grasp—the ashtray

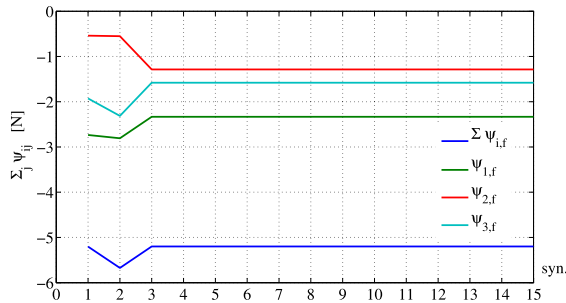
As second test case we consider the grasp of an ashtray. The hand configuration, the estimated position of the center of gravity  $CG$  of the object, and the contact points are rep-



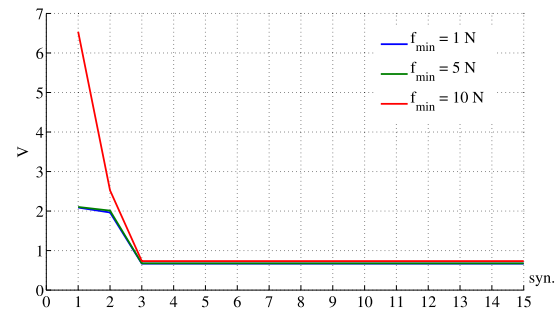
(a)  $\sum_i \psi_{i,f}$ ,  $\sum_i \psi_M$  and  $\sum_i \psi_m$  vs number of activated synergies



(a)  $V$  vs number of activated synergies, for different friction coefficient values.



(b)  $\psi_{i,f}$  vs number of activated synergies.



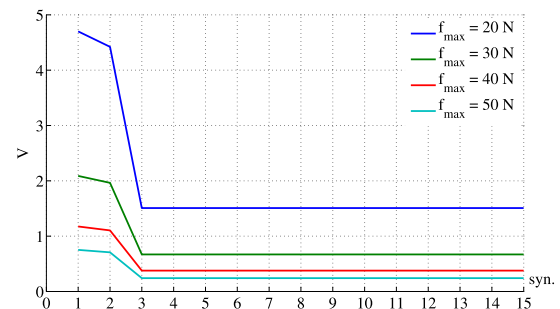
(b)  $V$  vs number of activated synergies, for different  $f_{\min}$  values.

**Fig. 11** (Color online) The cherry.  $\psi_{i,j}$  values as a function of the number of engaged synergies

resented in Fig. 4b. The contact parameters and the nominal stiffness values are the same employed in the previous case. This time,  $\text{rank}(G) = 6$ ,  $c = 18$  and, with reference to (12), (13), and (15),  $h = 12$ ,  $e = 12$ ,  $p = 0$ . As intuitive, since  $h = e < n$ , increasing the number  $s$  of synergies engaged results in a monotone decrease of the cost function (no matter the values of the grasping stiffness  $K$ ), until  $s = e$ , after which no improvement can be gained, as elicited from Fig. 14. All curves present a rapid decrease for  $1 \leq s \leq 2$ , then a lighter decrease for  $2 < s \leq 4$ , after which no practical improvement is registered. Also interesting is that synergy  $S_1$  represents the only “direction” along which we can obtain force-closure conditions by employing only a 1-dimensional subspace of  $\mathbb{R}^{15}$ , at least for nominal values of the parameters. No other synergy shows this property.

Moreover, it is worth noting that if the first four synergies are removed from the (kinematic) synergy manifold for the reference hand, no other subspace of dimension one, two, or three defined by arbitrarily combining the remaining  $S_5, \dots, S_{15}$  synergies is force-closure.

In subspaces of dimension four, only 1 combination—the sequence  $(S_5, S_6, S_7, S_{13})$ —over the 330 possible exhibits force-closure with quality metric ( $\|f_c\|_2$ ) 0.98. In subspaces of dimension five, 11 combinations over the 462 possible (2.38%) exhibit force-closure with mean quality metric of 0.99 and variance 0.21, the best sequence



(c)  $V$  vs number of activated synergies, for different  $f_{\max}$  values.

**Fig. 12** (Color online) The cherry.  $V$  sensitivities on  $\mu$ ,  $f_{\min}$  and  $f_{\max}$  parameters, for different numbers of activated synergies

being  $(S_5, S_6, S_7, S_{12}, S_{13})$  with a score of 0.68. In subspaces of dimensions six, 55 combinations over the 462 possible (11.9%) are force-closure with mean quality metric of 1.02 and variance 0.74, the best sequence being  $(S_5, S_7, S_9, S_{11}, S_{13})$  with a score of 0.48.

As intuitive, by engaging more synergies in the grasp force-closure is obtained more easily also without the first four synergies. However, with the first fundamental synergies engaged in an ordered fashion (see Figs. 14a–14b), the quality of the grasp is always by far better (the cost is much lower) than that registered with all the remaining higher-order synergies in arbitrary sequences.

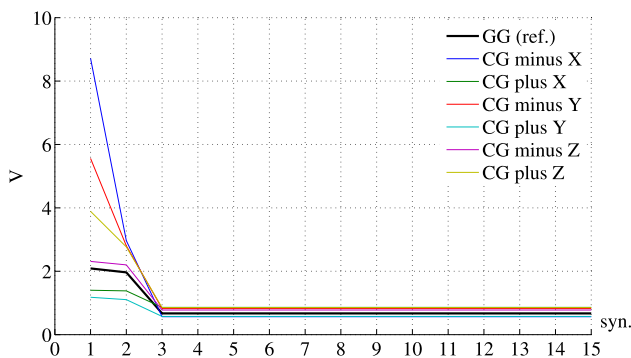


**Fig. 13** (Color online) The cherry.  $V$  sensitivities on object CG displacement

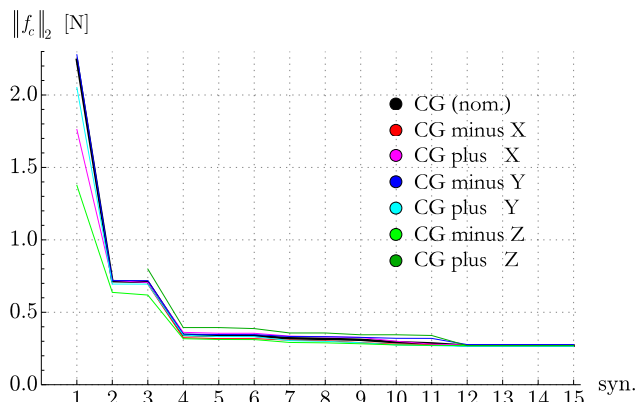
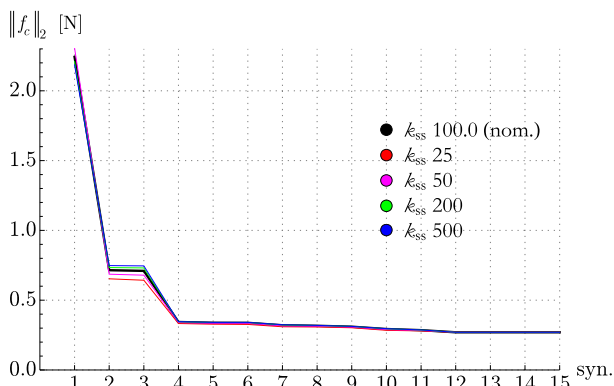
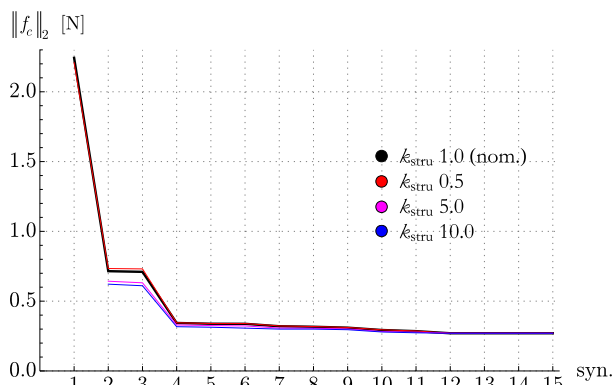


**Fig. 15** (Color online) The ashtray. Norm of the optimal contact force  $f$  w.r.t. the cost function  $\|f\|_2$ , with increasing number of synergies, sensitivity on object CG displacement



(a) Trends for variation of the steady-state gain  $k_{vss}$  (Nmm/rad).



(b) Trends for variation of the structural stiffness  $k_{stru}$  (N/mm).

**Fig. 14** (Color online) The ashtray. Norm of the optimal contact force  $f$  w.r.t. the cost function  $\|f\|_2$ , with increasing number of synergies

Figure 14 shows the results obtained moving the center of gravity  $CG$  in the  $x$ ,  $y$  and  $z$  (and consequently contact point positions and normal directions) as described for the cherry. Also in this case curve trends are robust with respect to variations of contact point location. We furthermore observe that in some configurations (for example, moving the

object in the  $z$  direction with a positive displacement), the grasp is not force closure if the number of engaged synergies is lower than 3.

Figure 16 shows the optimal contact force distribution found with respect to  $y$  minimizing  $\psi_{f_\infty}(y) = \|f(y)\|_\infty$  for the ashtray. The results show trends similar to those of Fig. 14.

In Figs. 14, 15 and 16 some of the curves are not defined when only one synergy  $S_1$  is engaged ( $k_{ss} = 25, 50$  and  $k_{stru} = 5, 10$ ), since in these cases force closure is not obtained. However, adding just one or two columns, e.g.  $S_2$  and  $S_3$ , solves already the problem.

If we select  $\Psi_\eta(y) = \|\eta\|_2$  as cost function, we obtain the trends depicted in Figs. 17a–17b.

$V$  cost function was evaluated, for different number of engaged synergies and for different values of the boundary parameters  $\mu$ ,  $f_{min}$  and  $f_{max}$ . Figure 18a summarizes the effect of the friction coefficient  $\mu$ , given  $f_{min} = 5$  N and  $f_{max} = 30$  N. For  $\mu = 1.0$  and  $\mu = 0.8$  the friction constraints are satisfied for all the considered synergies, however, decreasing the friction coefficient from  $\mu = 1.0$  to  $\mu = 0.8$  the cost function sensibly increases, especially when a small number of synergies are activated. Furthermore, decreasing the value of the friction coefficient, the minimum number of synergies necessary to satisfy the friction constraints in all the contact points increases: when  $\mu = 0.6$  we need at least four synergies (the  $V$  and curves are not defined for lower values), while when  $\mu = 0.4$  we need at least five synergies. Figures 18b and 18c summarize the  $f_{min}$  and  $f_{max}$  influence on  $V$ , with  $\mu = 0.1$ . The results are qualitatively similar to those observed for the precision grasp: relaxing the constraints, i.e. increasing  $f_{max}$  and decreasing  $f_{min}$ ,  $V$  decreases.

Finally, also for the ashtray the robustness of the observed  $V$  trends with respect to contact point displacements was analyzed: the results of the analysis are reported in Fig. 19.

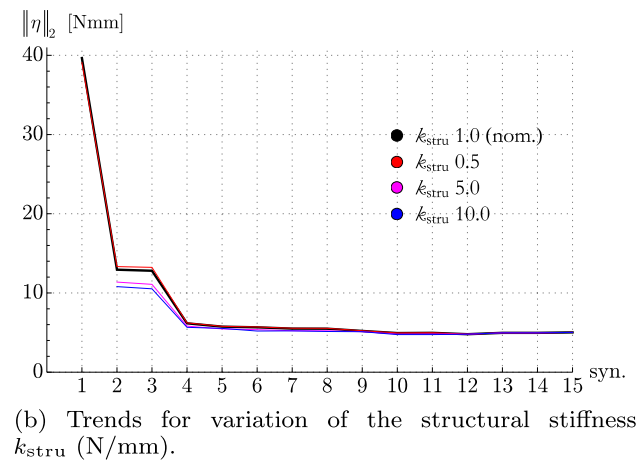
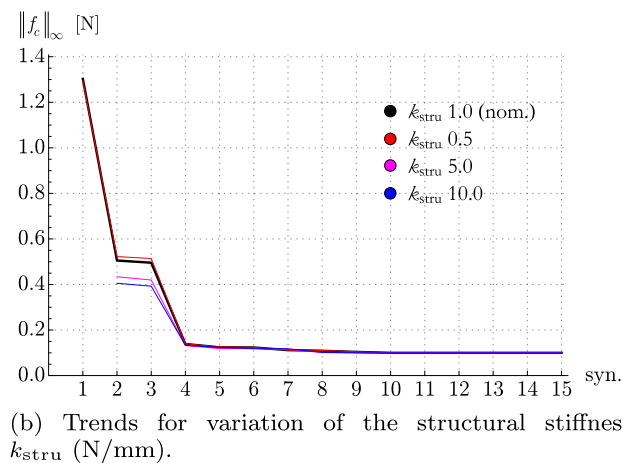
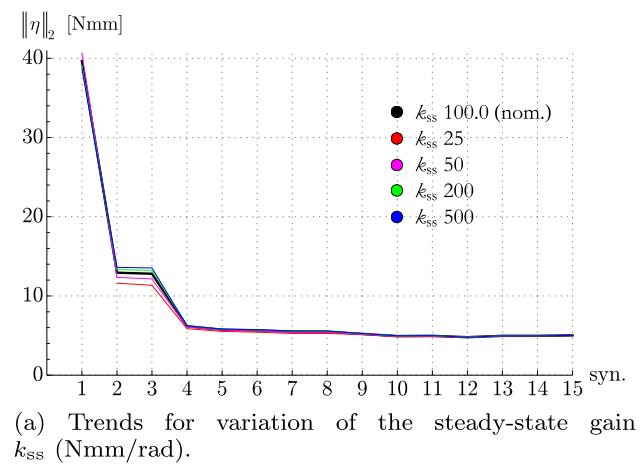
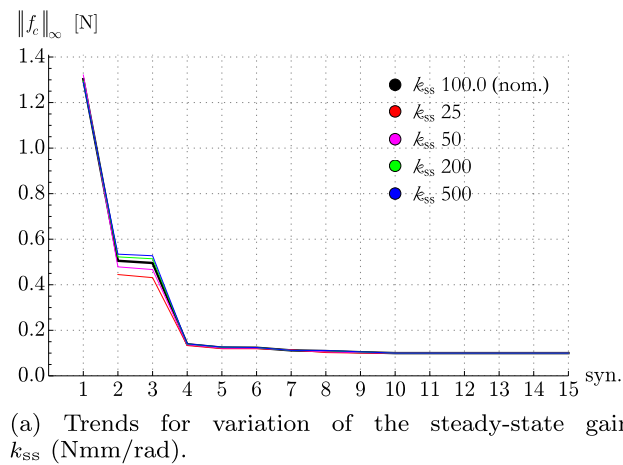


**Fig. 16** (Color online) The ashtray. Infinity norm of the optimal contact force  $f$  w.r.t. the cost function  $\|f\|_\infty$ , with increasing number of synergies

**Fig. 17** (Color online) The ashtray. Norm of the optimal synergistic force  $\eta = S^T \tau$  w.r.t. the cost function  $\|\eta\|_2$ , with increasing number of synergies

Also in this case the obtained  $V$  vs engaged synergies trends are robust with respect to small variation of the contact point positions.

## 6 Conclusion

The force decomposition and optimization problems in multiple whole-limb manipulation of hands with embodied synergies require an extension of existing analytical methods, and the consideration of compliance in the hand-object system.

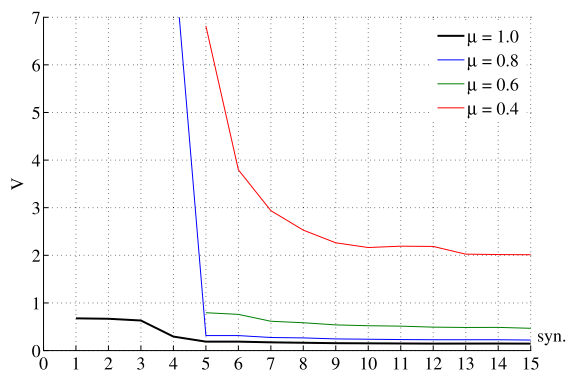
We have presented two numerical case studies to characterize the role of different postural synergies in the ability of the hand to obtain force-closure grasps. The two case studies addressed a precision grasp and a power grasp, respectively, and are to be considered representative of a number of similar experiments, which could not be reported for space limitations.

The main results obtained from our investigations can be summarized as follows.

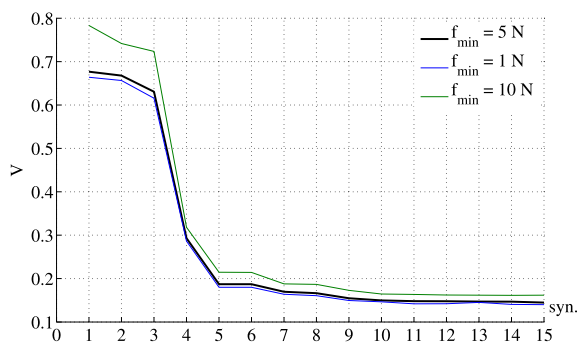
The force-closure property of grasps strongly depend on which synergies are used to control the hand. The first few synergies (the first one for the two case studies reported) are sufficient to establish force-closure. If the first few synergies are not actively controlled, force closure can only be obtained if many more DoFs (corresponding to higher-order synergies) are actuated.

A measure of the quality of the grasp (given in terms of the norm of contact forces needed to avoid slippage) is enhanced by increasing the number of actuated synergies, but only to a limited extent. No improvement is observed beyond the first three synergies in the precision grasp case, while continuous but small improvements are obtained in the whole-hand grasp case, until the dimension of the controllable force space is reached.

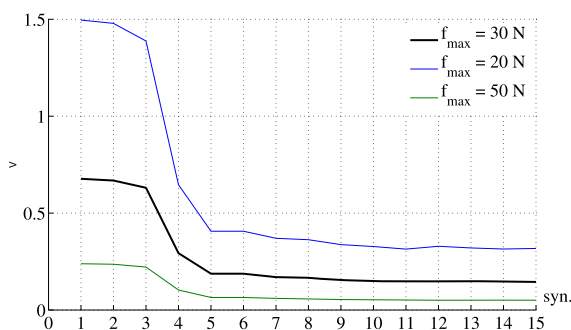
All the above results are consistently robust with respect to different values of stiffness parameters and contact point positions, which may reflect the uncertainty by which these parameters are known in human or robotic hand models,



(a)  $V$  vs number of activated synergies, for different friction coefficient values.



(b)  $V$  vs number of activated synergies, for different  $f_{\min}$  values.



(c)  $V$  vs number of activated synergies, for different  $f_{\max}$  values.

**Fig. 18** (Color online) The ashtray.  $V$  sensitivities on  $\mu$ ,  $f_{\min}$  and  $f_{\max}$  parameters, for different numbers of activated synergies

and/or the fact that grasp stiffness may be changed either voluntarily or not.

These results are consistent with the hypothesis that the first few postural synergies observed in grasp pre-shaping (Santello et al. 1998) are also crucial in grasping force optimization, when suitably translated from the kinematic configuration space where they have been observed, to the force domain through the procedures illustrated in this paper.

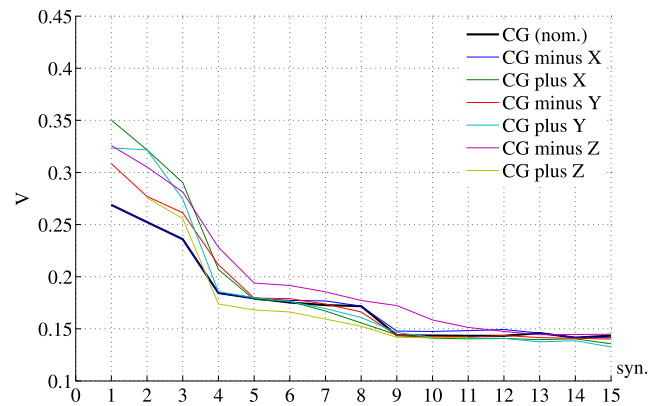


**Fig. 19** (Color online) The cherry.  $V$  sensitivities on object CG displacement

**Acknowledgements** Authors wish to gratefully acknowledge Marco Santello for the inspiring discussions and for providing experimental data and parameters. This work is supported by the European Commission under CP grant no. 248587, “THE Hand Embodied”, within the FP7-ICT-2009-4-2-1 program “Cognitive Systems and Robotics”.

## Appendix

According to standard conventions, we consider a fixed (palm) frame  $P = (O_p; x_p, y_p, z_p)$  and, for each finger in the hand, we attach a D.-H. frame  $S_{ij} = (O_{ij}; x_{ij}, y_{ij}, z_{ij})$  to its  $j$ th link, a local frame  $L_{ij} = (O_{lij}; x_{lij}, y_{lij}, z_{lij})$  to the center of the limb and a *normalized Gauss frame*  $C_{ij} = (C_{ij}; x_{cij}, y_{cij}, z_{cij})$  local to the surface of the fingertip, with its  $z$ -axis aligned with the outward normal. The frame attached to the object is  $E = (E; x_e, y_e, z_e)$ , with origin coincident with the center of gravity  $CG$ , i.e.,  $E \equiv CG$ .

Since only some of the fingers and/or some of the limbs in each finger may be in contact with the object at point  $c_{f_{ij}} \in \mathbb{R}^3$ , we define  $k$  sets of indices  $\nu(i)$ , ( $i = 1, \dots, k$ ), each one describing the connectivity of the  $i$ th finger with the object. In view of further analysis, we distinguish between corresponding points  $c_{f_{ij}}$  and  $c_{o_{ij}}$  on the finger and on the object, respectively. On the contrary, under the hypothesis of small relative elastic rotations, we confuse local frames at the contact point on the object and the limbs with the unique  $C_{ij}$ . In this analysis, the location of the contact points in space is assumed to be known, by either planning or sensing.

Let  $f_{ij} \in \mathbb{R}^{c_{ij}}$  be the components in the contact frame  $C_{ij}$  of force/torque that can be transmitted through the contact at point  $c_{f_{ij}}$ . Its dimension depends on the contact type, e.g.,  $c_{ij} = 3$  for Point Contact With Friction (PCWF),  $c_{ij} = 4$  for Soft Finger (SF), and its contribution to the actual wrench is characterized by the wrench basis  $H_{ij}^T$  (Featherstone 2008).

With reference to Fig. 1, and by employing the definition of the adjoint operator  $Ad_{(R,d)}$  given in Murray et al. (1994),

the contribution of the  $i$ th finger,  $j$ th limb to the components in  $P$  of the wrench  $w_e \in \mathbb{R}^6$  exerted on the object is given by

$${}^P w_{e_{ij}} = G_{ij} f_{ij}, \quad G_{ij} := \text{Ad}_{({}^{c_{ij}}R_p, d_{c_{ij}}^e)}^T H_{ij}^T \in \mathbb{R}^{6 \times c_{ij}}, \quad (43)$$

where  ${}^{c_{ij}}R_p$  is the rotation that aligns  $P$  onto  $C_{ij}$ , and  $d_{c_{ij}}^e$  is the vector from  $C_{ij}$  to  $E$ . Let  $\epsilon_{ij}$  be defined as follows

$$\epsilon_{ij} = \begin{cases} 1, & \text{if } j \in \nu(i), \\ 0, & \text{otherwise.} \end{cases} \quad (44)$$

Put  $f_i = [\epsilon_{i1} f_{i1}^T \cdots \epsilon_{in_i} f_{in_i}^T]^T \in \mathbb{R}^{c_i}$ , where  $c_i = \sum_{j \in \nu(i)} c_{ij}$ , and consider the contribution of the  $i$ th finger as

$${}^P w_{e_i} = G_i f_i, \quad G_i := [\epsilon_{i1} G_{i1} \cdots \epsilon_{in_i} G_{in_i}] \in \mathbb{R}^{6 \times c_i}. \quad (45)$$

Stacking (45) for each finger, we can write the global grasp matrix as

$${}^P w_e = G f, \quad G := [G_1 \cdots G_k] \in \mathbb{R}^{6 \times c}, \quad (46)$$

with  $c = \sum_{i=1}^k c_i$ .

Similarly, let  $\xi_{c_{o_{ij}}} \in \mathbb{R}^{c_{ij}}$  be the local components in the constrained directions at point  $c_{o_{ij}}$  due to a twist of the object  ${}^P \xi_e$ , with components in  $P$ . By setting  $\xi_{o_i} = [\epsilon_{i1} \xi_{c_{o_{i1}}}^T \cdots \epsilon_{in_i} \xi_{c_{o_{in_i}}}^T]^T \in \mathbb{R}^{c_i}$ , for the  $i$ th finger, and  $\xi_o = [\xi_{o_1}^T \cdots \xi_{o_k}^T]^T \in \mathbb{R}^c$ , for the whole hand, we can write by duality

$$\xi_o = G^T {}^P \xi_e, \quad G^T \in \mathbb{R}^{c \times 6}. \quad (47)$$

We now consider the relationships for the statics and kinematics of the fingers. By employing the D.-H. convention, the local components in the constrained directions of the contact point  $c_{f_{ij}}$  on the  $i$ th finger,  $j$ th limb, can be written as

$$\xi_{c_{f_{ij}}} = J_{ij} \dot{q}_i, \quad J_{ij} := H_{ij} \text{Ad}_{({}^{c_{ij}}R_p, d_{c_{ij}}^{o_{ij}})} J_{o_{ij}}(q_i), \quad (48)$$

where  $J_{o_{ij}} = [j_{i1} \cdots j_{ij} \ 0 \cdots 0] \in \mathbb{R}^{6 \times n_i}$ , with blocks defined as ( $1 \leq l \leq j$ )

$$j_{il} = \begin{cases} [z_{l-1}^T \ 0^T]^T, & \text{for prismatic } l\text{th joint;} \\ [(d_{o_{f_{ij}}}^{o_{f_{i,l-1}}})^T \ \hat{z}_{l-1} \ z_{l-1}^T]^T, & \text{for revolute } l\text{th joint.} \end{cases} \quad (49)$$

By stacking (48) for all the limbs on the  $i$ th finger that are actually in contact, and setting

$$\xi_{f_i} = [\epsilon_{i1} \xi_{c_{f_{i1}}}^T \cdots \epsilon_{in_i} \xi_{c_{f_{in_i}}}^T]^T \in \mathbb{R}^{c_i},$$

we obtain

$$\xi_{f_i} = J_i \dot{q}_i, \quad J_i := [\epsilon_{i1} J_{i1}^T \cdots \epsilon_{in_i} J_{in_i}^T]^T \in \mathbb{R}^{c_i \times n_i}. \quad (50)$$

Then, collecting the complete set velocities in twist  $\xi_f = [\xi_{f_1}^T \cdots \xi_{f_k}^T]^T \in \mathbb{R}^c$ , yields

$$\xi_f = J \dot{q}, \quad J := \text{Blockdiag}(J_1, \dots, J_k) \in \mathbb{R}^{c \times n}. \quad (51)$$

Finally, again by duality arguments, the map from the hand contact forces  $f$  to hand joint torques  $\tau$  is given by

$$\tau = J^T f, \quad J = \text{Blockdiag}(J_1^T, \dots, J_k^T) \in \mathbb{R}^{n \times c}. \quad (52)$$

### References

Bicchi, A. (1994). On the problem of decomposing grasp and manipulation forces in multiple whole-limb manipulation. *Robotics and Autonomous Systems*, 13(2), 127–147.

Bicchi, A. (1995). On the closure properties of robotic grasping. *The International Journal of Robotics Research*, 14(4), 319–334.

Bicchi, A. (2000). Hands for dextrous manipulation and robust grasping: a difficult road towards simplicity. *IEEE Transactions on Robotics and Automation*, 16(6), 652–662.

Bicchi, A., & Prattichizzo, D. (2000). Analysis and optimization of tendinous actuation for biomorphically designed robotic systems. *Robotica*, 18(1), 23–31.

Borgstrom, H., Batalin, M., Sukhatme, G., & Kaiser, W. (2010). Weighted barrier functions for computation of force distributions with friction cone constraints. In *2010 IEEE ICRA*, Anchorage, Alaska, USA (pp. 785–792).

Brown, C., & Asada, H. (2007). Inter-finger coordination and postural synergies in robot hands via mechanical implementation of principal component analysis. In *IEEE-RAS international conference on intelligent robots and systems* (pp. 2877–2882).

Buss, M., Hashimoto, H., & Moore, J. B. (1996). Dextrous hand grasping force optimization. *IEEE Transactions on Robotics and Automation*, 12(3), 406–418.

Chen, S. F. (2000). Conservative congruence transformation for joint and cartesian stiffness matrices of robotic hands and fingers. *The International Journal of Robotics Research*, 19(9), 835–847.

Cheung, V., d’Avella, A., Tresch, M., & Bizzi, E. (2005). Central and sensory contributions to the activation and organization of muscle synergies during natural motor behaviors. *The Journal of Neuroscience*, 25(27), 6419–6434.

Ciocarlie, M. T., & Allen, P. K. (2009). Hand posture subspaces for dexterous robotic grasping. *The International Journal of Robotics Research*, 28(7), 851–867.

Ciocarlie, M., Goldfeder, C., & Allen, P. (2007). Dimensionality reduction for hand-independent dexterous robotic grasping. In *Proceedings of the IEEE/RSJ international conference on intelligent robots and systems* (pp. 3270–3275).

Cutkosky, M., & Kao, I. (1989). Computing and controlling the compliance of a robotic hand. *IEEE Transactions on Robotics and Automation*, 5(2), 151–165.

Featherstone, R. (2008). *Rigid body dynamics algorithms*. Berlin: Springer.

Feldman, A. G., & Levin, M. F. (2009). The equilibrium-point hypothesis—past, present and future. *Advances in Experimental Medicine and Biology*, 629, 699–726.

- Friedman, J., & Flash, T. (2007). Task-dependent selection of grasp kinematics and stiffness in human object manipulation. *Cortex*, 43, 444–460.
- Grant, M., & Boyd, S. (2004). Cvx: Matlab software for disciplined convex programming (web page and software). <http://stanford.edu/boyd/cvx>.
- Grant, M., & Boyd, S. (2008). Graph implementations for nonsmooth convex programs. In *Recent advances in learning and control* (pp. 95–110).
- Hanafusa, H., & Asada, H. (1997). Stable prehension by a robot hand with elastic fingers. In *7th ISIR*, Tokyo.
- Joh, J., & Lipkin, H. (1991). Lagrangian wrench distribution for co-operating robotic mechanisms. In *IEEE conf. on robotics and automation*.
- Kao, I., Cutkosky, M., & Johansson, R. (1997). Robotic stiffness control and calibration as applied to human grasping tasks. *IEEE Transactions on Robotics and Automation*, 13(4), 557–566.
- Kim, K., Youm, Y., & Chung, W. (2002). Human kinematic factor for haptic manipulation: the wrist to thumb. In *Proceedings. 10th symposium on Haptic interfaces for virtual environment and tele-operator systems, 2002. HAPTICS 2002* (pp. 319–326).
- Lee, J., & Kunii, T. (1995). Model-based analysis of hand posture. *IEEE Computer Graphics and Applications*, 15(5), 77–86.
- Lin, J., & Wu, T. (2000). Modeling the constraints of human hand motion. *Urbana*, 51(61), 801.
- Linscheid, R., An, K., & Gross, R. (1991). Quantitative analysis of the intrinsic muscles of the hand. *Clinical Anatomy*, 4(4), 265–284.
- Mason, C.R., Gomez, J. E., & Ebner, T. J. (2001). Hand synergies during reach-to-grasp. *Journal of Neurophysiology*, 86(6), 2896–2910.
- Murray, R. M., Li, Z., & Sastry, S. (1994). *A mathematical introduction to robotic manipulation*. Boca Raton: CRC Press.
- Prattichizzo, D., & Trinkle, J. C. (2000). Grasping. In *Springer Handbook of Robotics*. Berlin: Springer.
- Santello, M., Flanders, M., & Soechting, J. F. (1998). Postural hand synergies for tool use. *The Journal of Neuroscience*, 18(23), 10105–10115.
- Toh, K. C., Todd, M., & Tutuncu, R. (1999). Sdpt3—a matlab software package for semidefinite programming. *Optimization Methods & Software*, 1, 545–581.
- Youm, Y., Holden, M., & Dohrmann, K. (1977). *Finger ray ratio study* (Technical Report on Wrist Project).



**M. Gabbicini** received the Laurea degree (cum laude) and the Ph.D. both from the University of Pisa, Pisa, Italy, in 2000 and 2006, respectively. During his Ph.D. he was a visiting scholar at the GearLab, The Ohio State University, Columbus, from 2003 to 2004. Since 2001, he has been doing research at the Department of Mechanical, Nuclear and Production Engineering, University of Pisa. In 2006, he also joined the Interdepartmental Research Center “E. Piaggio”. He is currently a faculty member of the

Department of Mechanical, Nuclear and Production Engineering (DIMNP). He teaches Robotics, Applied Mechanics and Biomechanics at the University of Pisa, Faculty of Engineering. His main research interests are in the field of theory of gearing, geometrical methods in robotics and in the areas of dynamics, kinematics and control of complex mechanical systems.



**A. Bicchi** received the “Laurea” degree in Mechanical Engineering from the University of Pisa in 1984, and the Doctoral degree from the University of Bologna in 1989. After a post-doctoral fellowship at the Artificial Intelligence lab, Massachusetts Institute of Technology, he joined the Faculty of Engineering in the University of Pisa in 1990. He is Professor of Systems Theory and Robotics in the Department of Electrical Systems and Automation (DSEA) of the University of Pisa and the Director of the Interdepartmental Research Center “E. Piaggio” of the University of Pisa, where he has been leading the Automation and Robotics group since 1990. His main research interests are in: dynamics, kinematics and control of complex mechanical systems, including robots, autonomous vehicles, and automotive systems; haptics and dexterous manipulation; theory and control of nonlinear systems, in particular hybrid (logic/dynamic, symbol/signal) systems. Antonio Bicchi is a Fellow of IEEE, and elected Chair of the Conference Editorial Board of IEEE Robotics and Automation Society.



**D. Prattichizzo** is Professor of Robotics at the Dipartimento di Ingegneria dell’Informazione of the University of Siena. Laurea degree in Electronics Engineering and Ph.D. degree in Robotics and Automation from the University of Pisa in 1991 and 1995, respectively. In 1994, Visiting Scientist at the MIT Artificial Intelligence Lab. Since 2002 Associate Co-editor of two books by STAR, Springer Tracks in Advanced Robotics, Springer (2003, 2005). Guest editor of the special issue on Robotics and Neuroscience of the Brain Research Bulletin (2008). Since 2007 Associate Editor in Chief of the IEEE Transactions on Haptics. Since 2006 Chair of the Italian Chapter of the IEEE Society of Robotics and Automation. Awarded with the 2009 IEEE RAS Chapter of the Year Award. Since 2006 Vice-chair for special issues and workshops of the IEEE Technical Committee on Haptics. From 2003 to 2007, Associate Editor of the IEEE Trans on Robotics and IEEE Trans. on Control Systems Technologies. Member of the Editorial Board of many Conferences on Control and Robotics. His main research interests are in haptics, grasping and dexterous manipulation, control of robots and mechanical systems, computer vision and geometric control theory.



**M. Malvezzi** is Assistant Professor of Mechanics and Mechanism Theory at the Dipartimento di Ingegneria dell’Informazione of the University of Siena. Laurea degree in Mechanical Engineering from the University of Florence in 1999 and Ph.D. degree in Applied Mechanics from the University of Bologna in 2003. Her main research interests are in control of mechanical systems, robotics, autonomous vehicle localization, multibody dynamics, haptics, grasping and dexterous manipulation.